Experimental characterization and mitigation of turbulence induced signal fades within an ad hoc FSO network

Joaquin Perez,[1,*] Stanislav Zvanovec,[2] Zabih Ghassemlooy[1] and Wasiu O. Popoola[3]

[1]*Optical Communications Research Group, Faculty of Engineering and Environment, Northumbria University, NE1 8ST, Newcastle Upon Tyne, UK*

[2]*Department of Electromagnetic Field, Czech Technical University in Prague, 2 Technicka, 16627 Prague, Czech Republic*

[3]*School of Engineering and Built Environment, Glasgow Caledonian University, G4 0BA, Glasgow, UK*

[*]*joaquin.perez@northumbria.ac.uk*

Abstract: Optical beams propagating through the turbulent atmospheric channel suffer from both the attenuation and phase distortion. Since future wireless networks are envisaged to be deployed in the ad hoc mesh topology, this paper presents the experimental laboratory characterization of mitigation of turbulence induced signal fades for two ad hoc scenarios. Results from measurements of the thermal structure constant along the propagation channels, changes of the coherence lengths for different turbulence regimes and the eye diagrams for partially correlated turbulences in free space optical channels are discussed. Based on these results future deployment of optical ad hoc networks can be more straightforwardly planned.

OCIS codes: (060.2605) Free-space optical communication; (010.1330) Atmospheric turbulence; (060.4510) Optical communications.

References and links

1. Z. Ghassemlooy, W. Popoola, and S. Rajbhandari, *Optical Wireless Communications: System and Channel Modelling with MATLAB* (CRC Press., Boca Raton, 2012).
2. "fSONA unveils 2.5-Gbps free-space optical systems," in *Lightwave Online,* (2012).
3. S. Nauerth, F. Moll, M. Rau, C. Fuchs, J. Horwath, S. Frick, and H. Weinfurter, "Air-to-ground quantum communication," Nat. Photonics **7**(5), 382–386 (2013).
4. E. Ciaramella, Y. Arimoto, G. Contestabile, M. Presi, A. D'Errico, V. Guarino, and M. Matsumoto, "1.28 terabit/s (32x40 Gbit/s) WDM transmission system for free space optical communications," IEEE J. Sel. Areas Comm. **27**(9), 1639–1645 (2009).
5. E. Leitgeb, M. Gebhart, and U. Birnbacher, "Optical networks, last mile access and applications," J. Opt. Fiber Commun. Rep. **2**, 56–85 (2005).
6. M. N. Smadi, S. C. Ghosh, A. A. Farid, T. D. Todd, and S. Hranilovic, "Free-space optical gateway placement in hybrid wireless mesh networks," J. Lightwave Technol. **27**(14), 2688–2697 (2009).
7. A. O. Aladeloba, A. J. Phillips, and M. S. Woolfson, "Improved bit error rate evaluation for optically pre-amplified free-space optical communication systems in turbulent atmosphere," IET Optoelectron. **6**(1), 26–33 (2012).
8. L. Dordova and O. Wilfert, "Calculation and comparison of turbulence attenuation by different method," Radioengineering **19**, 162–163 (2010).
9. L. C. Andrews and R. L. Phillips, *Laser Beam Propagation through Random Media,* II ed. (SPIE Press, Washington, 2005).
10. W. Gappmair, "Further results on the capacity of free-space optical channels in turbulent atmosphere," IET Commun. **5**(9), 1262–1267 (2011).
11. M. A. Khalighi, N. Schwartz, N. Aitamer, and S. Bourennane, "Fading reduction by aperture averaging and spatial diversity in optical wireless systems," J. Opt. Commun. Netw. **1**(6), 580–593 (2009).
12. T. A. Tsiftsis, H. G. Sandalidis, G. K. Karagiannidis, and M. Uysal, "Optical wireless links with spatial diversity over strong atmospheric turbulence channels," IEEE Trans. Wirel. Comm. **8**(2), 951–957 (2009).
13. G. Yang, M.-A. Khalighi, S. Bourennane, and Z. Ghassemlooy, "Approximation to the sum of two correlated gamma-gamma variates and its applications in free-space optical communications," IEEE Wireless Commun. Lett. **1**(6), 621–624 (2012).

#198825 - $15.00 USD Received 3 Oct 2013; revised 20 Dec 2013; accepted 21 Dec 2013; published 4 Feb 2014

14. S. Kaneko, T. Hamai, and K. Oba, "Evaluation of a free-space optical mesh network communication system in the Tokyo metropolitan area," J. Opt. Netw. **1**, 414–423 (2002).
15. M. A. Kashani, M. Safari, and M. Uysal, "Optimal relay placement and diversity analysis of relay-assisted free-space optical communication systems," J. Opt. Commun. Netw. **5**(1), 37–47 (2013).
16. X. Yang, "Availability-differentiated service provisioning in free-space optical access networks," J. Opt. Netw. **4**(7), 391–399 (2005).
17. Z. Hu, P. Verma, and J. J. Sluss, Jr., "Improved reliability of free-space optical mesh networks through topology design," J. Opt. Netw. **7**(5), 436–448 (2008).
18. S. D. Milner, J. Llorca, and C. C. Davis, "Autonomous reconfiguration and control in directional mobile ad-hoc networks," IEEE Circuits Syst. Mag. **9**(2), 10–26 (2009).
19. J. Libich, S. Zvanovec, and M. Mudroch, "Mitigation of time-spatial influence in free-space optical networks utilizing route diversity," Proc. SPIE **8246**, 82460O (2012).
20. S. Hippler, F. Hormuth, D. J. Butler, W. Brandner, and T. Henning, "Atmosphere-like turbulence generation with surface-etched phase-screens," Opt. Express **14**(22), 10139–10148 (2006).
21. C. Wilcox and S. Restaino, "A New Method of Generating Atmospheric Turbulence with a Liquid Crystal Spatial Light Modulator," in *New Developments in Liquid Crystals*, G. V. Tkachenko, ed. (InTech, 2009), pp. 71–92.
22. Z. Ghassemlooy, H. Le Minh, S. Rajbhandari, J. Perez, and M. Ijaz, "Performance analysis of ethernet/fast-ethernet free space optical communications in a controlled weak turbulence condition," J. Lightwave Technol. **30**(13), 2188–2194 (2012).
23. W. K. Pratt, *Laser Communication Systems*, I ed. (John Wiley & Sons, Inc., New York, 1969).
24. A. Kolmogorov, ed., *Turbulence*, Classic Papers on Statistical Theory (Wiley-Interscience, New York, 1961).
25. A. M. Obukhov, "Structure of the temperature field in turbulent flow," Izv. Akad. Nauk. SSSR Ser.Ser. **13**, 58–96 (1949).
26. S. Corrsin, "On the spectrum of isotropic temperature fluctuations in an isotropic turbulence," J. Appl. Phys. **22**(4), 469–473 (1951).
27. G. R. Osche, *Optical Detection Theory for Laser Applications*, I ed. (Wiley-Interscience, 2002).
28. Z. Ghassemlooy, W. O. Popoola, S. Gao, J. I. H. Allen, and E. Leitgeb, "Free-space optical communication employing subcarrier modulation and spatial diversity in atmospheric turbulence channel," IET Optoelectron. **2**(1), 16–23 (2008).
29. M. Uysal, J. T. Li, and M. Yu, "Error rate performance analysis of coded free-space optical links over gamma-gamma atmospheric turbulence channels," IEEE Trans. Wirel. Comm. **5**(6), 1229–1233 (2006).
30. H. Moradi, H. H. Refai, and P. G. LoPresti, "Switch-and-stay and switch-and-examine dual diversity for high-speed free-space optics links," IET Optoelectron. **6**(1), 34–42 (2012).
31. S. Zvanovec, J. Perez, Z. Ghassemlooy, S. Rajbhandari, and J. Libich, "Route diversity analyses for free-space optical wireless links within turbulent scenarios," Opt. Express **21**(6), 7641–7650 (2013).
32. Y. Guowei, M. Khalighi, and S. Bourennane, "Performance of receive diversity FSO systems under realistic beam propagation conditions," in *Proc. of the 2012 8th Int. Symp. Commun. Syst. Netw. Digital Signal Process. (CSNDSP)*, (2012), pp. 1–5.
33. J. Jaeshin and W. Sunghong, "Comparative study on cooperative communications in the upper layers at ad-hoc networks," in *2013 15th Int. Conf. Adv. Commun. Technolo. (ICACT)* (2013), pp. 133–137.
34. J. Perez, Z. Ghassemlooy, S. Rajbhandari, M. Ijaz, and H. L. Minh, "Ethernet FSO communications link performance study under a controlled fog environment," IEEE Commun. Lett. **16**(3), 408–410 (2012).
35. J. A. Louthain and J. D. Schmidt, "Anisoplanatism in airborne laser communication," Opt. Express **16**(14), 10769–10785 (2008).

1. Introduction

Optical wireless communications (OWC) is a complementary technology to the radio frequency (RF) wireless systems, which has gained momentum mainly offering considerably higher transmission rates as well as inherent security [1]. Several successful demonstrations and trials of free space optical (FSO) communication links, part of OWC systems, have been reported with commercially available FSO systems offering full duplex transmission at 2.5 Gb/s over a link span of 5 km [2]. Another recent successful trial involved a secure free-space quantum key distribution communications between an aircraft travelling at 290 km/h at an altitude of 20 km and a ground station [3]. An FSO link capable of delivering data rates in the Tb/s range by employing dense wavelength-division multiplexing (DWDM) in the license-free spectral bands has also been reported in [4]. In their demonstration, 1.28 Tb/s (using a 32-channel DWDM each running at 40 Gb/s) of transmission over an optical wireless link of around 210 m above the rooftops in Pisa, Italy was reported. Such high-bandwidth OWC technologies are very attractive for a number of applications including the last-mile access

#198825 - $15.00 USD Received 3 Oct 2013; revised 20 Dec 2013; accepted 21 Dec 2013; published 4 Feb 2014

networks [5], the backbone segments of mobile infrastructures connecting cellular base station for 4G mobile long term evolution traffic, and ad hoc hybrid networks [6].

FSO links experience performance degradation due to the scattering (caused by snow, fog, rain, pollution, sand and dust particles), absorption, and atmospheric turbulences [7, 8]. The variation of the air refractive index as a result of non-homogeneities in the temperature and pressure of the atmosphere leads to random variations of the light intensity, both in space and time, along the propagation path and subsequently at the receiver plane [9]. The intensity fluctuations, also referred to as the scintillation noise, can dramatically degrade the performance of intensity modulation with direct detection (IM/DD) FSO link even in clear weather conditions, as evident from both experimentally and analytically derived results shown in [10].

The degradation of an outdoor FSO link's performance in terms of the optical signal fades due to the atmospheric turbulence is very well reported. For example, the effect of scintillation induced fading as a consequence of the turbulence events over the optical signal has been described by means of theoretical modelling in [10–13]. In [13], an analytical approach has been adopted to investigate the impact of fading correlation on the system BER performance by means of extending the α-β distribution to the case of multiple diversity by approximating the sum of arbitrarily correlated multiple Gamma-Gamma random variables. The analytical results obtained have demonstrated substantial improvement of FSO links over 2 and 5 km when using multiple apertures separated by at least 1.41 cm at the transmitter side.

Regarding FSO based networks, in [14] a mesh optical network topology with route diversity is introduced to balance the network traffic load by exploiting multiple routes within the network. Experiments undertaken in the Tokyo area based on a mesh configuration (9 FSO communication devices spread over approximately 1 km^2) have demonstrated that an improvement of up to ~5% of the reliability of the worst available route was attainable by employing route diversity within the network. In [15], a detailed theoretical analysis and optimization of serial and parallel nodes together with further quantification of diversity advantages relating to the number of relays and channel parameters are presented. In [16] availability-differentiated networking schemes supporting two classes of service availability - low-availability services and by high-availability services - are proposed for short and long range links in FSO mesh networks. This approach was analysed for mesh topologies that resemble the street block structure in urban areas, and was tested over 30 randomly generated topologies. The methodology for the topological design of FSO mesh networks and hybrid RF/FSO gateways are analyzed in [6] and [17], respectively. Moreover, an autonomous topology reconfiguration as dynamic redirection of point-to-point links using heuristic algorithms for creating new topologies and pointing, acquisition and tracking of links and physical interactions between network nodes was proposed in [18] for optical wireless networks. It is clear that research and technological progress within FSO based network topologies requires novel characterization together with practical implementation and verification of basic approaches in a wider context. This is true especially for the mutual influence between paths within networks, which are affected by spatially non-homogeneous atmospheric scattering, like time-space dependent turbulence, and others.

In practice, assessment of the FSO network depends on gathering measured signal data over a long period of time. The cost and time implication of this process explains why there are few such real-life data published in the literature. One such long-term measurements was carried out at the Czech Technical University, Prague as outlined in [19]. Their measurements show that the route diversity scheme can further enhance the availability of FSO links.

In order to assess the impact of turbulence-like atmosphere on optical beam propagation under repeatable controlled environment there are a number of precise approaches including surface-etched phase-screens, and liquid crystal spatial light modulators [20, 21]. In this paper we study the atmospheric turbulence effect on a FSO based ad hoc network using a dedicated

#198825 - $15.00 USD Received 3 Oct 2013; revised 20 Dec 2013; accepted 21 Dec 2013; published 4 Feb 2014

indoor FSO atmospheric channel emulator. The emulator enable us to perform comprehensive assessment of the FSO link under a controlled environment and to obtain results that are complementary to the data gathered from outdoor links [22].

The rest of the paper is organized as follows: Section II gives the theoretical background of the atmospheric turbulence and its impact on the FSO topologies. In Section III, the experimental set-up that is used in the laboratory to study the atmospheric turbulence effect on an FSO based ad hoc network is presented. The key findings are introduced and discussed in Section IV with concluding remarks given in Section V.

2. Atmospheric turbulence theoretical background

2.1 Statistical models

The random fluctuation of the atmospheric temperature along the optical beam propagation path results in variation of the atmospheric refractive index [23]. In order to characterize the atmospheric turbulence we have focused on the index of refraction structure parameter C_n^2. Dissipation mechanism for temperature non-homogeneities was introduced by extension of the Kolmogorov theory of structure functions [24] (models for velocity fluctuations) to the thermal fluctuations by Obukhov [25] and Corrsin [26] by C_n^2 as a function of pressure P_{as}, wavelength λ and temperature T given by:

$$C_n^2 = \left(86\times10^{-6}\frac{P_{as}}{T_e}\right)^2 C_T^2, \text{at } \lambda = 850\text{nm}, \tag{1}$$

where the temperature structure constant C_T^2 is related to the 2/3 power law of temperature variation along the path. C_T^2 can be derived from the general definition of structure function D_T associated with the random processes as [25, 26]:

$$D_T = \left\langle (T_1 - T_2)^2 \right\rangle = \begin{cases} C_T^2 l_0^{-4/3} L_p^2 & for \quad 0 < L_p < l_0 \\ C_T^2 L_p^{2/3} & for \quad l_0 < L_p < L_0 \end{cases}, \tag{2}$$

where T_1 and T_2 are the temperatures measured at two points separated by the distance L_p. Values of C_n^2 could vary from 10^{-17} $m^{-2/3}$ up to 10^{-12} $m^{-2/3}$ and the strength of scintillation is a function of the C_n^2 profile and beam parameters [9]. Due to the random nature and presence of non-linear mixing of observable quantities, the turbulent media are generally not easy to describe from first principles [27]. The two most popular statistical models for optical intensity variation under various turbulence strengths in a single channel are the log-normal and Gamma-Gamma models [9]. These models have been extensively investigated in [28]. The probability distribution function (pdf) of Gamma-Gamma and log-normal models for describing irradiance fluctuation can be expressed by the following, respectively [29]:

$$f(I) = \frac{2(\alpha\beta)^{\frac{(\alpha+\beta)}{2}}}{\Gamma(\alpha)\Gamma(\beta)} I^{\frac{\alpha+\beta}{2}-1} K_{\alpha-\beta}\left(2\sqrt{\alpha\beta I}\right), I > 0, \tag{3}$$

$$f(I) = \frac{1}{\sqrt{2\pi}\sigma_I I}\left\{\frac{\left(\ln(I/I_0) + \sigma_I^2/2\right)^2}{2\sigma_I^2}\right\}, I > 0, \tag{4}$$

where α and β are the effective numbers for large- and small-scale turbulence eddies in the scattering environment, respectively. σ_1^2 is the variance of the log amplitude irradiance [30], I and I_0 denotes irradiance (intensity of the optical wave) and its mean value for the case with no turbulence, $\Gamma(\cdot)$ stands for the Gamma function and $K_n(\cdot)$ is the modified Bessel function of the 2nd kind of order n.

#198825 - $15.00 USD Received 3 Oct 2013; revised 20 Dec 2013; accepted 21 Dec 2013; published 4 Feb 2014

The error performance for the case of FSO links with spatial diversity has been derived for three different linear combining techniques at the receiver part – maximal ratio combining, equal gain combining, and selection combining in [28].

The case of two FSO parallel links each under the influence of different turbulence conditions was investigated experimentally in [31]. The measurements revealed an enhancement in the received optical power level under a particular signal fade when the receiver is able to switch to the second less affected channel. Contrary to analytical assumptions from [28], the modified Student's t-distribution with *N*-degree of freedom (corresponding to the number of channels) was applied to isolated turbulence within measured diversity channels (isolated either in both channels or just one channel) in [31]. A joint statistic combiner sampled the entire received signal through multiple branches and selecting the highest irradiance level combined received power is described by the density function as [31]:

$$p = \frac{\Gamma\left(\frac{N+1}{2}\right)}{\sigma_I \sqrt{N\pi}\,\Gamma\left(\frac{N}{20}\right)}\left[\frac{N+\left(\frac{I-I_0}{0.1\sigma_I}\right)^2}{N}\right], \tag{5}$$

where N is the number of FSO channels and σ_1^2 is the irradiance variance. Regarding analyses of correlated and un-correlated channels, approximation of the sum of Gamma-Gamma random variables by α-μ distribution was proposed in [13] to evaluate the receiver performance of the dual space diversity FSO systems, as:

$$p(r) = \frac{\alpha\mu^{\mu} r^{\alpha\mu-1}}{\hat{r}^{\alpha\mu}\Gamma(\mu)} \exp\left(-\mu\frac{r^{\alpha}}{\hat{r}^{\alpha}}\right), r < 0, \tag{6}$$

where $\alpha > 0$, $\mu = \left(E\left\{R^{\alpha}\right\}\right)^2 / Var\left\{R^{\alpha}\right\} > 0$ is the inverse of the normalized variance R^{α}, $\hat{r} = \sqrt[\alpha]{E\left\{R^{\alpha}\right\}}$, $E\{.\}$ denotes the expected value, and $Var(.)$ is the variance. According in Gamma-Gamma model [9], I is considered as the product of two independent Gamma random variables, X and Y, that represent the irradiance fluctuations arising from large- and small-scale turbulence, respectively. We approximate the Gamma-Gamma channel fading I by the α-μ random variable that it is denoted by R.

A good match between the analytical model, given by (6) and simulation results for Gamma-Gamma random variables especially for the (1 × 2) system with uncorrelated fading has been reported in [13] and validated via analytical BER tests. In other cases, this approximation slightly overestimated the receiver performance. It was shown that uncorrelated fading, under the mean turbulence regime, is related to the wavelength and separation of the receivers. Therefore there is a trade-off between the receiver aperture and the receivers separation distance, which defines the performance of the FSO link with regard to its spatial correlation [32].

2.2 Network topologies

It is envisaged that future wireless networks will be based on ad hoc topologies with multiple retransmit nodes rather than the classical systems with many base stations. Considering the mesh network shown in Fig. 1 as an example, the traffic from Node A to Node B (or in opposite direction) can be redirected away from the most affected links C-B via other nodes, thus substantially improving availability of the network.

#198825 - $15.00 USD Received 3 Oct 2013; revised 20 Dec 2013; accepted 21 Dec 2013; published 4 Feb 2014

Typically, nodes can be used in proactive or reactive modes. Comparison of the cooperative MAC protocols, the routing protocols and the transport protocols, all of which support cooperative and ad hoc communications and numerical comparisons of three cooperative MAC protocols with reactive helper node selection mechanisms were presented in [33]. In this paper the focus is more on the physical layer. In contrast to analytical studies, very few experimental results have been published for ad hoc optical networks. The evaluation of an FSO mesh network communication system in the Tokyo metropolitan area was introduced in [14]. This was the first report on ascertaining the effectiveness of routing in an FSO mesh network. It was derived, that the availability of optical nodes increases by up to ~5% when the route diversity mechanism is adopted within the network. Another experimental campaign using three FSO links, a radio link and two meteorological stations was set up in the campus of the Czech Technical University (CTU) in Prague [19]. The outage statistic within this simple network was found to be best approximated by a generalized extreme value distribution, defined by:

$$f\left(x|k,\mu,\sigma\right)=\left(\frac{1}{\sigma}\right)\exp\left(-\left(1+k\frac{\left(x-\mu\right)}{\sigma}\right)^{-\frac{1}{k}}\right)\left(1+k\frac{\left(x-\mu\right)}{\sigma}\right)^{-1-\frac{1}{k}}, \qquad (7)$$

with specific values of location μ, scale σ and k shape parameters derived from measurements, see [19]. Nevertheless, outdoor measurement campaigns carried out for FSO networks so far have not provided a complete set of needed tested cases. Thus, there is a need for additional laboratory measurements to fully assess the design and implementation of such network topologies.

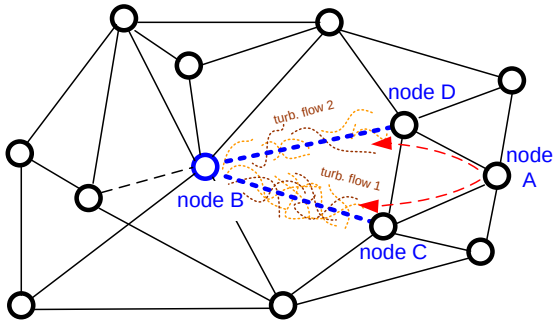

Fig. 1. Mesh topology and the network path equivalent to the FSO path under study (dashed line).

3. Laboratory experimental set-up

The emulator used for carrying out the experimental work is an indoor atmospheric chamber/test-bed at Northumbria University, UK. This indoor test-bed, see Fig. 2, had previously been used to successfully characterize and study the link attenuation and scintillations for a one-to-one direct line-of-sight FSO link [34].

However, the experimental work and analyses outlined in previous sections necessitated changing the set-up in order to investigate, in a small scale, an ad hoc FSO network with a routing technique. To achieve this, the following two scenarios will be considered based on Fig. 1. The first set-up is to replicate a segment of the ad hoc network where Node C transmits to Nodes D and B. In this set-up, the link segment between Nodes B and C is degraded by turbulence while the link segment between Nodes D and C is not. This is implemented by using a plexiglass wall located within the atmospheric chamber to create two paths as shown in Fig. 3(a). The second set-up is to replicate a situation in which a hub, says Node B, is routing optical signals to the receiving Nodes D and C for instance. In this

#198825 - $15.00 USD Received 3 Oct 2013; revised 20 Dec 2013; accepted 21 Dec 2013; published 4 Feb 2014

scenario, the link paths (Node D - to - Node B and Node C – to – Node B) are both affected by a varying degree by the atmospheric turbulence. This was implemented by using two separate optical sources and a glass wall in order to create two separate channels with a varying degree of turbulence strength as illustrated in Fig. 3(b).

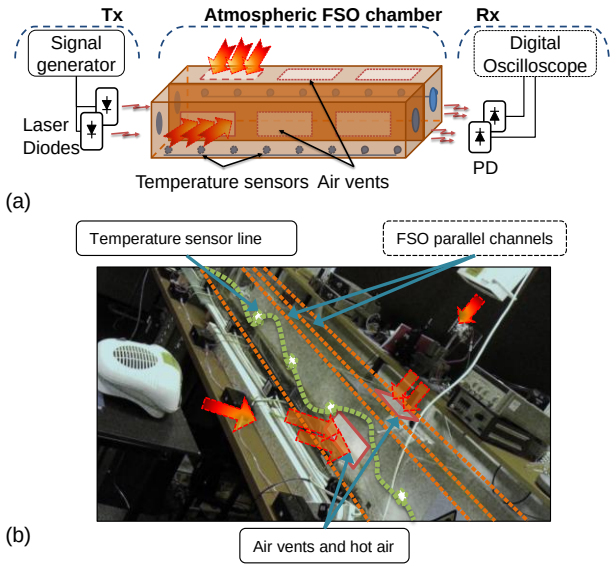

Fig. 2. (a) Block diagram of the laboratory turbulence chamber implemented for measurements and (b) annotated photograph of the atmospheric chamber used and the laboratory set-up, main components underlined.

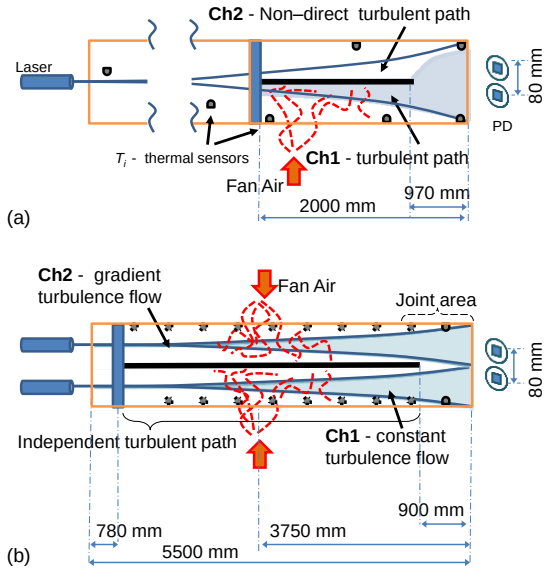

Fig. 3. Block diagrams of beam and turbulence interaction as measured in experimental laboratory for: (a) split beam, and (b) multiple channels FSO system

The controlled indoor atmospheric channel test-bed is made from combinations of modular 5.5 m × 0.3 m × 0.3 m glass chambers. The turbulence strength within the chamber is defined by the thermal fluctuations inside the chamber. Moreover, a number of air vents located along the length of the chamber (i.e. line-of-sight path) allow us to blow hot and cold

#198825 - $15.00 USD Received 3 Oct 2013; revised 20 Dec 2013; accepted 21 Dec 2013; published 4 Feb 2014

air from external sources in directions that are perpendicular to the propagating optical beam within the chamber. A variation in the turbulence strength is achieved by adjusting the temperature and air flow of the fan heater sources, thus ensuring a temperature gradient of >6° C. The turbulence strength is adjusted by the strength of fan heaters and how far they are positioned from the air vents. In these experiments we considered a range of temperatures from 20°C to 60°C. The temperature at different locations along the chamber was measured and recorded every second by a network of 19 temperature sensors positioned within the chamber; see Fig. 2(b), each with a measurement span of −55°C to + 125°C and a resolution of 0.1°C. The measured temperatures are used to determine the temperature structure constant, as depicted in Fig. 2(b).

The first experimental set-up depicted by Fig. 3(a) uses an 830 nm laser diode with built-in circular collimating lens, 50 MHz electrical bandwidth and 10 mW optical power. For the second set-up, shown in Fig. 3(b), a 632 nm laser diode with 10 mW optical power and 50 MHz electrical bandwidth is employed to allow configuration of two FSO channels. The emitted optical beams from laser sources are intensity modulated using OOK-NRZ signal format with 1 Mbit/s line-rate and 250 mV_{pp} electrical signal amplitude. The receiver front-end consists of a Silicon PIN photodiode with 150 MHz bandwidth, 0.8 mm^2 active area and responsivities of 0.38 A/W and 0.39 A/W at 830 nm and 670 nm, respectively. The regenerated electrical signal is then captured using a high-frequency digital sampling oscilloscope. The captured signal thereafter is processed off-line using mathematical analysis software to obtain the following performance metrics: BER, *Q*-factor, SNR and eye diagrams.

4. Results and discussions

4.1 The first scenario

The first measurement was performed for the configuration of split beam transmission, as described in Fig. 3(a). The laser beam at 830 nm broaden in the first half of the chamber is passed through the plexiglass perpendicularly placed slab (shown in blue in Fig. 3) and then split into two beams by the lengthwise plexiglass. The split beams propagate through two ~1 m length channels, one with turbulence and one without. This is followed by a common ~1 m long path with turbulence.

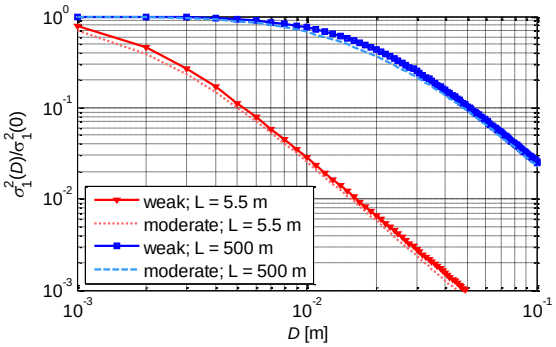

Fig. 4. Aperture averaging derived for 5.5 m channel (red curves) and 500 m channel (blue curves) for weak and moderate turbulence

The fact that only a small fraction of the path is affected differently by turbulence, results in much reduced scintillation effect. The diversity of co-propagating beams (in terms of ratio of the detected power levels) varied by about 0.2 dB and did not exceed 0.4 dB even in the case of high turbulence regimes (i.e. $C_n^2 > 10^{-11}$ $m^{-2/3}$). When the effective area of the photodetector was considered in order to reduce the turbulence influence in one channel, experimental measurements showed only marginal improvement ($\sigma_1^2(0)/\sigma_1^2(D) = 0.7$). The

#198825 - $15.00 USD Received 3 Oct 2013; revised 20 Dec 2013; accepted 21 Dec 2013; published 4 Feb 2014

difference of Rytov variance between both receiving channels, derived from optical signal fluctuations expressed as Rytov variance ratio ($\sigma_{R2}^2/\sigma_{R1}^2$), was decreased due changes in the turbulences level from 0.9 to 0.1. A real outdoor analogy of this observation will occur when aperture averaging (with a diameter of 5 mm) is applied in case of 5.5 m long optical link or averaging over a diameter of 30 mm in case of 500 m long link, see derived dependences in Fig. 4.

4.2 The second scenario - channels with partially intersect path

In the second case, the channel 2 was under the influenced of a constant weak turbulence regime (measured Rytov variance in the channel was kept at <0.16), while the turbulent flow circulating from channel 1 to the area of intersection (and partially to the path of channel 1) was gradually increased from 10^{-13} up to 10^{-11} $m^{-2/3}$ (values enumerated from temperature measurement via Eq. (1)). The measurement environment is shown in Fig. 3(b). This deployment corresponds to the blue depicted network segment from Fig. 1, where the interconnecting Node B serves as a routing hub to several nodes. At first, the data captured using the temperature sensors was analyzed in order to obtain the relationship between measured turbulence regimes and temperature changes along propagating optical paths. From these statistics, the correlation of C_n^2 profile within the channels was observed to change from 0.1068 up to 0.4896 in line with the increase in the turbulence level in the channel 1.

The next interesting parameter analyzed for the ad hoc network is the change in the transverse coherence distance (note for the distance from axis of propagation when modulus of the complex degree of coherence to 1/e of axis value), which is useful for determination of the proper transversal separation between detectors in order to ensure receiving uncorrelated signals. Note other expression for beam separation is set by the scintillation anisoplanatic distance [35]. Values of the traverse coherence distance were derived from measured distributions of thermal structure parameter C_T^2 (recalculated on distribution of C_n^2) along the optical beams according to [9]:

$$\rho_0 = \left[1.45k^2 \int_0^{L_p} C_n^2(x)\,dx \right]^{-3/5}. \tag{8}$$

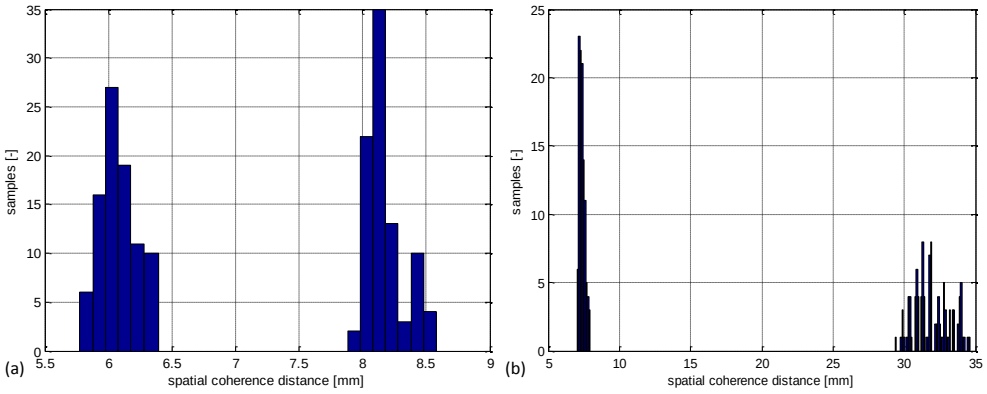

Fig. 5. Derived empirical histograms of spatial coherence distance determined from measured C_T^2 profiles for cases: (a) similar C_n^2 in channels and (b) one order different C_n^2 in the channels

Figure 5 shows typical example of derived empirical histograms against the spatial coherence distances for both channels with similar C_n^2, see Fig. 5(a) and for channels with different values of C_n^2 (i.e. one order higher in on channel) see, Fig. 5(b).

Due to varying the degree of turbulence strength, we noticed a decrease in the mean received power, which depends on the mean index of refraction structure parameter measured

#198825 - $15.00 USD Received 3 Oct 2013; revised 20 Dec 2013; accepted 21 Dec 2013; published 4 Feb 2014

along the channel 1. This feature can be clearly quantified in terms of the diversity gain dependence on C_n^2 as illustrated in Fig. 6. In this case the diversity gain represents an improvement of the optical signal when it is retransmitted through the channel 1 with a constant weak turbulence regime in comparison to the signal received in the channel 2 with gradual increase in the turbulence level. For a better insight into the turbulence influence on transmitted signal in both channels, the blue curves in Fig. 6 represent Rytov variances derived from the received optical data signals for increased values of C_n^2 in the channel 1.

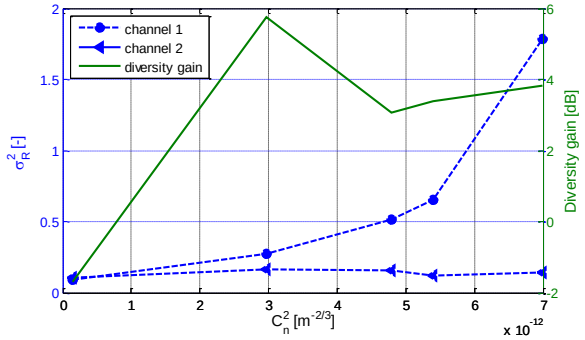

Fig. 6. Measured dependence of Rytov variance in both channels and the link diversity gain against C_n^2 measured in the channel 1

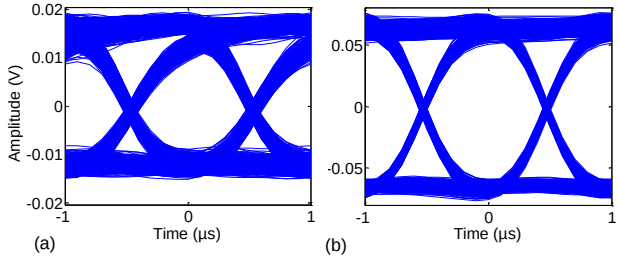

Fig. 7. Eye diagrams for the initial turbulence scenario for: (a) channel 1 (C_n^2 = 10^{-13} m$^{-2/3}$), and (b) channel 2 received signals

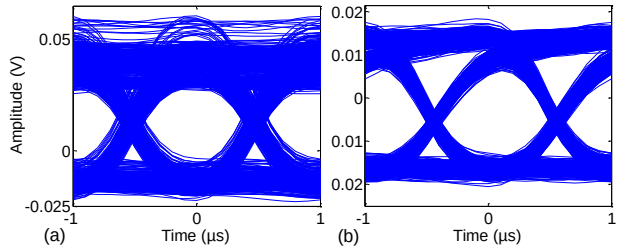

Fig. 8. Eye diagrams for final turbulence scenario for: (a) channel 1 (C_n^2 = 10^{-11} m$^{-2/3}$), and (b) received signals in channel 2

Distortions in channel 1 caused by the weak and moderate turbulence regimes are then illustrated by means of measured eye diagrams as in Figs. 7 and 8, respectively. In this case the channel 1 is clearly affected by the improvement of turbulent atmospheric channel, measured by C_n^2, denoting a smaller eye opening as in Fig. 8(a). Analyzing the values of *Q*-factor derived from the eye diagrams, the channel 1 varies from 8.46 in Fig. 7(a) to 5.52 in Fig. 8(a). On the other hand, the channel 2 is only affected for the moderate turbulence regime because of the intersection area. This is clearly depicted in the eye opening and the related *Q*-factor values of 19.14 and 7.59 in Figs. 7(b) and 8(b), respectively for the channel

#198825 - $15.00 USD Received 3 Oct 2013; revised 20 Dec 2013; accepted 21 Dec 2013; published 4 Feb 2014

2. Therefore, in contrast to two independent co-propagating optical beams in the two channels as in the first test scenario, for the second test scenario, Fig. 3(b), the measured scintillation is more than two orders of magnitude higher. It has to be mentioned, even though it is impossible within any measurement procedure to acquire strictly ergodic values of random variables (temperature distributions within the channels etc.), it has been confirmed the specific deviation of ad hoc segments statistics from the strict theoretical assumptions.

5. Conclusion

The characterization of scintillation index, empirical histograms, eye diagrams and structure coefficient statistics within an ad hoc FSO network in the presence of turbulence was presented. The derived results from test scenarios of ad hoc network has demonstrated that it is more effective to adopt the aperture averaging scheme than employing multiple receiver to reduce the influence of turbulence on the propagating optical beam over shorter path length. On the contrary for the fades of segments where majority of link paths experience different turbulence regimes, the fluctuations of received signals can be substantially reduced either by retransmitting the information over the diversity path or by adopting the less effective scheme of aperture averaging. The joint measurement campaign has led to novel results for utilization of the routing diversity scheme to improve the design of optical wireless ad hoc networks topology.

Acknowledgments

This research is supported by the EU COST ICT Action IC1101 - Optical Wireless Communications - An Emerging Technology (OPTICWISE) and by the MEYS Czech Republic grant LD12058.

#198825 - $15.00 USD Received 3 Oct 2013; revised 20 Dec 2013; accepted 21 Dec 2013; published 4 Feb 2014